Published online 9 March 2010

Nucleic Acids Research, 2010, Vol. 38, No. 12 ***4173–4181***
doi:10.1093/nar/gkq153

Twisting of the DNA-binding surface by a β-strand-bearing proline modulates DNA gyrase activity

Tung-Ju Hsieh[1,2], Tien-Jui Yen[1], Te-Sheng Lin[1,2], Hsun-Tang Chang[2], Shu-Yun Huang[2], Chun-Hua Hsu[3], Lynn Farh[4] and Nei-Li Chan[1,2,*]

[1]Institute of Biochemistry and Molecular Biology, College of Medicine, National Taiwan University, Taipei City 100, [2]Institute of Biochemistry, National Chung Hsing University, Taichung City 402, [3]Department of Agricultural Chemistry, College of Bio-Resources and Agriculture, National Taiwan University, Taipei City 106 and [4]Department of Chemical Biology, National Pingtung University of Education, Pingtung City, Pingtung 900, Taiwan

Received October 23, 2009; Revised and Accepted February 22, 2010

ABSTRACT

DNA gyrase is the only topoisomerase capable of introducing (−) supercoils into relaxed DNA. The C-terminal domain of the gyrase A subunit (GyrA-CTD) and the presence of a gyrase-specific 'GyrA-box' motif within this domain are essential for this unique (−) supercoiling activity by allowing gyrase to wrap DNA around itself. Here we report the crystal structure of *Xanthomonas campestris* GyrA-CTD and provide the first view of a canonical GyrA-box motif. This structure resembles the GyrA-box-disordered *Escherichia coli* GyrA-CTD, both adopting a non-planar β-pinwheel fold composed of six seemingly spirally arranged β-sheet blades. Interestingly, structural analysis revealed that the non-planar architecture mainly stems from the tilted packing seen between blades 1 and 2, with the packing geometry likely being defined by a conserved and unusual β-strand-bearing proline. Consequently, the GyrA-box-containing blade 1 is placed at an angled spatial position relative to the other DNA-binding blades, and an abrupt bend is introduced into the otherwise flat DNA-binding surface. Mutagenesis studies support that the proline-induced structural twist contributes directly to gyrase's (−) supercoiling activity. To our knowledge, this is the first demonstration that a β-strand-bearing proline may impact protein function. Potential relevance of β-strand-bearing proline to disease phenylketonuria is also noted.

INTRODUCTION

Type II DNA topoisomerases (Topos) are ubiquitous enzymes that catalyze ATP-dependent passage of one DNA duplex (termed the 'transported' or T-segment) through a transient double-stranded break in another duplex (termed the 'gate' or G-segment) (1,2). Such activity alters DNA topology, allowing these enzymes to solve topological conflicts arising during cellular DNA transactions (3). Although all type II Topos possess duplex passage activity, resultant changes in DNA topology depend upon how two DNA segments are captured and recognized as the T- and G-segments, respectively. Conventional type II Topos, including bacterial Topo IV and eukaryotic Topo II, resolve mainly pre-existing DNA crossovers, leading to the relaxation of supercoils or decatenation of interlinked chromosomes (4,5). Interestingly, the majority of bacteria possess a specialized type II enzyme named DNA gyrase that can actively shape DNA curvature and pump (−) supercoils into the relaxed DNA molecule (6). In particular, the DNA segment that extends from the active site-bound G-segment can be chirally wrapped by gyrase into a (+) supercoil-like intramolecular DNA crossover to favor *in cis* presentation of the T-segment. Subsequent passage of the T-segment through the cleaved G-segment inverts the sign of crossover, producing net (−) supercoils on DNA (7).

The gyrase holoenzyme is a tetramer composed of two GyrA and two GyrB subunits, each possessing distinct functional modules (1,8). Among them, the GyrA C-terminal domain (GyrA-CTD) exhibits chiral DNA-wrapping activity and plays an essential role in defining the functional uniqueness of gyrase (9,10). Deletion of GyrA-CTD abolishes gyrase's ability to catalyze (−)

*To whom correspondence should be addressed. Tel: +886 2 2356 2214; Fax: +886 2 2391 5295; Email: nlchan@ntu.edu.tw; neilichan@gmail.com

supercoiling reaction and converts gyrase into a conventional type II Topo which simply performs relaxation and decatenation (10), demonstrating the direct participation of this domain in the *in cis* T-segment presentation. Moreover, the GyrA-CTD harbors a positively charged and gyrase-specific 'GyrA-box' motif required for both DNA-wrapping and supercoiling activities of gyrase (11,12).

Structural analysis revealed that the *Escherichia coli* GyrA-CTD (EcGyrA-CTD) adopts a six-bladed and seemingly spiral-shape 'β-pinwheel' fold (13), highlighted by the non-planar orientation between the two terminal β-sheet blades (blades 1 and 6). This feature presumably presents a right-hand curved DNA binding surface along the structural perimeter suitable for inducing chiral DNA-wrapping. However, it remains controversial whether planarity of the GyrA-CTD has an effect on gyrase's hallmark DNA-wrapping and (−) supercoiling activities. Rather than adopting the non-planar architecture seen in EcGyrA-CTD, the *Borrelia burgdorferi* GyrA-CTD (BbGyrA-CTD) is a flat β-pinwheel, with its GyrA-box residues apparently involving in the planar packing between the terminal blades 1 and 6 (14). Because the GyrA-box of BbGyrA-CTD deviates significantly from the consensus sequence, it has been argued that the flat BbGyrA-CTD may be a structural outlier, and those GyrA-CTDs with a canonical GyrA-box would resemble the non-planar EcGyrA-CTD (13). In addition, this crucial motif is completely disordered in the EcGyrA-CTD structure; thus, the influence of the canonical GyrA-box on overall structural curvature remains unclear (1,13). Most surprisingly, the homologous but functionally divergent CTD of *Bacillus stearothermophilus* Topo IV (BsParC-CTD) exhibits a similar non-planar overall shape as the EcGyrA-CTD (15). Given that ParC-CTD possesses only DNA-binding activity but is incompetent in performing handed DNA-wrapping (4,14), therefore the structural determinant that allows EcGyrA-CTD to wrap DNA and the molecular basis for the functional distinction between gyrase and Topo IV have remained enigmatic.

To resolve these outstanding controversies, we determined the crystal structure of *Xanthomonas campestris* GyrA-CTD (XcGyrA-CTD) and revealed for the first time the structure of the canonical GyrA-box motif. Not only does this new structure strengthen the non-planar architecture of canonical GyrA-CTD β-pinwheel, structural analysis further led to the identification of a conserved and unusual β-strand-bearing proline that may affect the structural planarity of the β-pinwheel domain. The impact of this structurally unique proline on gyrase's (−) supercoiling activity was illustrated by site-directed mutagenesis studies, which represents the first example of a β-strand-bearing proline with functional significance. Our finding suggests that particular attention should be paid to the structural and functional consequences of conserved β-strand-bearing prolines in other proteins. A potential medical relevance of this study is also discussed.

MATERIALS AND METHODS

Protein preparation

Using a standard PCR-based cloning strategy, the coding region of the *X. campestris* GyrA-CTD (XcGyrA-CTD, residues 531–899) was generated and inserted in-frame with a C-terminal His-tag into a modified pET-21b vector. SeMet-labeled XcGyrA-CTD was produced in methionine-auxotrophic *E. coli* strain B834(DE3) using previously reported procedures (16), and purified by immobilized Ni^{2+}-affinity and size-exclusion chromatography to homogeneity. Purified protein was stored in gel-filtration buffer (25 mM Tris-HCl pH 7.5, 300 mM NaCl, 1 mM EDTA and 1 mM dithiothreitol) and concentrated to ~20 mg/ml for crystallization.

The coding regions of full-length *E. coli* GyrB, GyrA and GyrA-CTD (EcGyrA-CTD, residues 533–850) were generated by standard PCR-based strategy and individually inserted in-frame with a C-terminal His-tag into a modified pET-21b vector. QuikChange™ mutagenesis method (Stratagene) was applied to these vectors to replace residues Pro636 and Arg580 of the full-length GyrA and EcGyrA-CTD with Ala to allow the expression of mutant proteins GyrA(P636A), GyrA(R580A), EcGyrA-CTD(P636A) and EcGyrA-CTD(R580A). The wild-type and all mutant proteins were produced in *E. coli* strain Rosetta(DE3)pLysS, with 0.5 mM IPTG induction for 14 h at 20°C. Recombinant proteins were purified using the procedure described above for XcGyrA-CTD and stored under the same buffer condition. Functional gyrases were reconstituted by mixing purified GyrA (or mutant GyrA) and GyrB subunits in 1:1.2 molar ratio, followed by size-exclusion chromatography to obtain the $(GyrA)_2(GyrB)_2$ tetramer.

X-ray crystallography

Initial crystallization trials were performed with commercially available kits (Hampton Research, USA) using the hanging-drop vapor-diffusion method. Crystals of selenomethionyl XcGyrA-CTD were obtained at 277 K using 2 μl protein solution and 2 μl different reservoir solutions consisting of 200 mM ammonium sulfate, 100 mM Bis-Tris pH 5.2–5.9 and 25–29% (v/v) PEG 3350. Crystals for data collection were cryoprotected by increasing the ethylene glycol concentration of the reservoir to 15–20% and then immediately flash-frozen in liquid nitrogen. Multi-wavelength anomalous diffraction (MAD) datasets were collected from a single SeMet-labeled crystal at two different wavelengths (Se inflection and high remote) on beamline SP12B2 (SPring8, Japan) and processed using the HKL2000 software suite (17). Data from each wavelength were indexed according to the same crystal orientation matrix but integrated and scaled independently. Experimental phases of XcGyrA-CTD were obtained at 2.6 Å using the MAD method implemented in the program SOLVE (18), and were further improved and extended to 2.2 Å by a better-diffracting native dataset collected on beamline BL13B1 (NSRRC, Taiwan). The resulting experimental electron-density maps were of good quality

Table 1. Summary of crystallographic analysis for XcGyrA-CTD

Protein	XcGyrA-CTD		
Space group	*P*1		
Unit cell dimensions			
a (Å)	52.5		
b (Å)	59.0		
c (Å)	74.4		
α (°)	78.9		
β (°)	79.7		
γ (°)	69.7		
Data collection	Se-edge	Se-remote	Native
Wavelength (Å)	0.97960	0.96430	1.00000
Resolution (Å)	30.0–2.6	30.0–2.6	30.0–2.19
Observed reflections	91 857	92 777	151 223
Unique reflections	23 401	23 634	40 325
Completeness (last shell)[a] (%)	93.1 (66.2)	96.3 (78.8)	96.5 (95.2)
Multiplicity	3.9	3.9	3.8
R_{sym} (last shell)[a,b] (%)	6.5 (20.0)	6.2 (20.0)	4.4 (10.9)
Refinement			
Resolution range (Å)			25.6–2.2
No. of reflection in working set (test set)			38 300 (2022)
R_{cryst} (last shell)[a,c] (%)			22.3 (23.2)
R_{free} (last shell)[a] (%)			27.5 (32.6)
r.m.s.d from ideal			
Bond lengths (Å)			0.013
Bond angles (°)			1.723
Ramachandran analysis[d] (%)			
Favored regions			93.5
Generously allowed regions			6.5
Outliers			None

[a]Statistics for data from the resolution shell of 2.25–2.19 Å.
[b]$R_{sym} = (\Sigma\Sigma \mid I_{hkl} - \langle I \rangle \mid)/(\Sigma I_{hkl})$, where the average intensity $\langle I \rangle$ is taken overall symmetry equivalent measurements and I_{hkl} is the measured intensity for any given refection.
[c]$R_{cryst} = (\Sigma \parallel F_o \mid - k \mid F_c \parallel)/(\Sigma \mid F_o \mid)$.
[d]Categories were defined by Swiss-Pdbviewer v.4.0. All non-glycine residues are included for this anlaysis.

(Supplementary Figure S1), which allowed RESLOVE (19–21) to build initial models. The programs O (22) and REFMAC5 (23) were then used for rounds of manual model rebuilding and refinement, respectively. Data collection and refinement statistics were summarized in Table 1.

Topo I readout of protein-induced DNA-wrapping

Wild-type or mutant EcGyrA-CTDs (38.4–307.2 nM) were incubated with (−) supercoiled plasmid pUC119 (300 ng; 9.6 nM) in 15 µl buffer that contained 35 mM Tris–HCl, pH 8.0, 72 mM KCl, 5 mM $MgCl_2$, 5 mM DTT, 5 mM spermidine, 0.01% bovine serum albumin, 6.7% glycerol, 0.1 mM EDTA, and 1 Weiss unit T4 DNA ligase. After 1 h, 16°C incubation, 0.5 unit of *calf thymus* DNA Topo I was added and the mixtures were incubated for another 4 h. The reaction was stopped by adding 5 µl of stopping buffer (6% SDS, 30% glycerol, 10 mM EDTA, bromophenol blue) and incubation at 42°C for 10 min. DNA products were resolved by 1% agarose gel electrophoresis in 0.5× TBE at 4 V/cm for 16 h at 4°C. After EtBr staining, the topoisomer bands were quantified and normalized, and plotted and fitted to Gaussian curves using SigmaPlot2001. The signs of the topoisomers were established by resolving the DNA samples with an agarose gel that contained chloroquine (0.6 µg/ml). The linking-number change per EcGyrA-CTD produced on the circular DNA plasmid was estimated by the quotient of the peak shifts in Gaussian curves divided by the increase in the molar ratio of protein. The experimental parameters used in this assay were based on previous studies and our experimental refinement (13,24).

DNA supercoiling assay

DNA supercoiling activity was assayed with relaxed pUC119 as a substrate. Reactions (20 µl) were carried out in a buffer containing 35 mM Tris–HCl (pH 7.5), 24 mM KCl, 6 mM $MgCl_2$, 6.5% glycerol, 100 µg/ml BSA, 5 mM DTT, 1 mM ATP, with 300 ng relaxed pUC119 and either wild-type or mutant *E. coli* gyrases at 37°C for 30 min. Following reaction termination and deproteination, DNA products were resolved by 1% agarose gel electrophoresis in 0.5× TBE at 4 V/cm for 16 h, and stained with EtBr.

RESULTS AND DISCUSSION

Structural determination

The crystal structure of XcGyrA-CTD was solved by the MAD technique using selenomethionine-labeled protein and refined to a final R_{work} and R_{free} of 22.3 and 27.5%, respectively, with good stereochemistry (Table 1). The final model consists of two protein molecules per asymmetric unit (designated chain A and B), with chain A containing 313 residues and chain B 305 residues. The two crystallographically independent XcGyrA-CTD chains are highly similar (with an r.m.s.d. value of 0.61 Å over 295 equivalent Cα atom pairs), except for the region between residues 560–575. Whereas the corresponding electron density allowed interpretation of this region as an ordered loop in chain A (Supplementary Figure S1B), residues 560–567 were disordered in chain B. Because residues 560–565 comprise the functionally significant GyrA-box motif (11,12), the structure of XcGyrA-CTD chain A is of particular functional importance by revealing for the first time the spatial arrangement of the canonical GyrA-box within the context of the β-pinwheel fold (Figure 1). Given that chain A represents a more complete model for XcGyrA-CTD, it was used for all subsequent structural analyses.

XcGyrA-CTD is non-planar with uneven axial rises between adjacent blades

Unlike the atypical GyrA-box motif of BbGyrA-CTD which interacts extensively with blade 6 residues (Figure 2B) (14), the DNA-binding canonical GyrA-box of XcGyrA-CTD exists as a fully exposed surface loop that links blades 1 and 6 without contacting surrounding residues (Figures 1A and 2, Supplementary Figure S1B). Although higher B-factors are associated with GyrA-box residues due to the lack of direct interactions, the spatial location of the GyrA-box motif is defined by the presence of anchoring residues from both sides. Specifically,

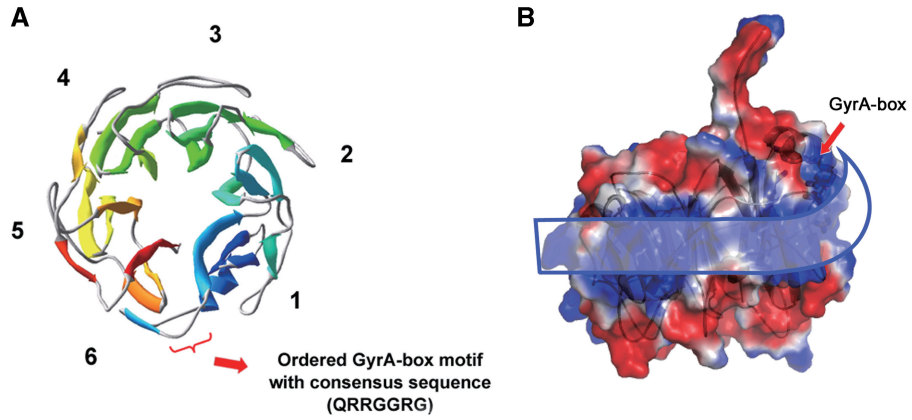

Figure 1. Overall structure and surface electrostatic feature of XcGyrA-CTD. (**A**) Ribbon representation of the XcGyrA-CTD β-pinwheel. Blades 1–6 are numbered along the sequence and rainbow-colored with the N-terminus in blue and the C-terminus in red. The position of the canonical GyrA-box motif (residues 560–565) is indicated. (**B**) Side view of the surface electrostatic property of XcGyrA-CTD. Basic, acidic and uncharged surface regions were colored blue, red and white, respectively. A basic patch suitable for DNA-binding can be identified along the structural perimeter. The upward curving ribbon highlights the curvature of this positively charged surface.

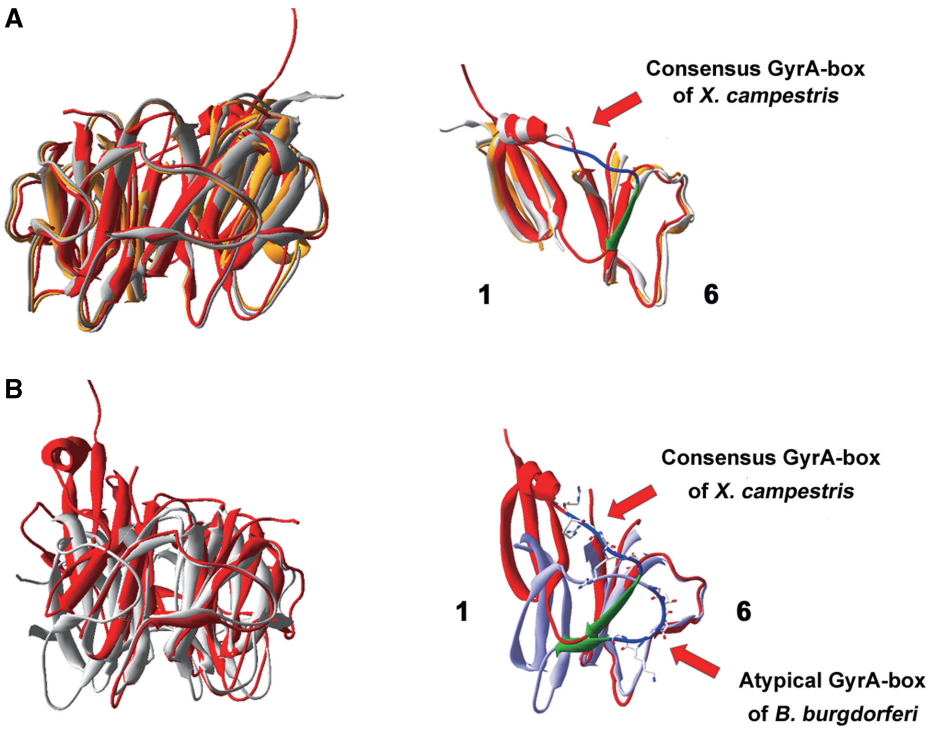

Figure 2. Structural comparisons among XcGyrA-CTD, EcGyrA-CTD (13) and BbGyrA-CTD (14). (**A**) Left: superimposition of the XcGyrA-CTD (chains A and B are colored red and orange, respectively) with the non-planar EcGyrA-CTD (grey, PDB-ID: 1zi0). Right: the spatial location of the canonical GyrA-box motif (residues 560–565) of XcGyrA-CTD is highlighted in blue. Residues 566–570 of XcGyrA-CTD form a β-strand (green) and become an integral part of blade 6. (**B**) Left: superimposition of XcGyrA-CTD chain A (red) with the planar BbGyrA-CTD (grey). Right: the spatial location of the GyrA-box motifs (blue) and the 'Velcro' structures of XcGyrA-CTD (red) and BbGyrA-CTD (light blue) are very different. Residues 566–570 of XcGyrA-CTD and the corresponding residues of BbGyrA-CTD are colored green.

residues 554–559 form an α-helix whose position is specified by other blade 1 residues and residues 566–570 fold into a β-strand to become an integral part of blade 6. While residues 555–575 appear to latch blades 1 and 6 together by forming a Velcro-like closure, the XcGyrA-CTD closely resembles the non-planar EcGyrA-CTD (13) rather than the flat BbGyrA-CTD (14) (Figure 2). It appears that the Velcro closure does not constrain the β-pinwheel structure into a flat ring, and that GyrA-CTDs with the consensus GyrA-box motif more likely adopt a non-planar architecture.

Unexpectedly, although the non-planar XcGyrA-CTD and EcGyrA-CTD did not superimpose well with the flat BbGyrA-CTD, the quality of structural alignment was

Table 2. Axial displacement[a] between the centroids of two consecutive β-pinwheel blades

Centroid displacement (Å)[b]	BbGyrA-CTD	XcGyrA-CTD (this work)	EcGyrA-CTD
Blade 1	1.713	5.435[b]	4.393[b]
Blade 2	NA[a]	1.310	1.362
Blade 3	0.932	1.910	2.100
Blade 4	2.738	1.303	1.706
Blade 5	0.665	1.159	2.480

[a]The 'centroid displacement' provides a direct measurement of the axial rise of each blade along the β-pinwheel's central shaft. The B2–B3 pair of BbGyrA-CTD (14) was used as the reference for this calculation, thus displacement for blade 2 is not available for this structure.
[b]In an ideal situation, no significant axial rise between adjacent blades is expected for a flat β-pinwheel ring, and the measured centroid displacements should be close to zero. In the real case, however, the exact location of a blade centroid is determined by the spatial distribution of constituting atoms of a blade. Therefore, given the sequence and structural variations between blades, it is anticipated that the calculated values would deviate from zero. As shown in the table, an average centroid displacement of ~1.5 Å was observed for BbGyrA-CTD. Because BbGyrA-CTD exhibits a flat overall shape, the average centroid displacement (~1.5 Å) of this structure may conveniently serve as an experimentally determined confidence level (or noise level) for judging whether two adjacent blades from the non-planar XcGyrA-CTD and EcGyrA-CTD (13) structures are in-plane (flat, with no significant axial rise) or out-of-plane (with meaningful axial rise). Two adjacent blades are said to be significantly non-planar only when the calculated axial displacement exceeds ~3.0 Å, which is two times higher than the average noise level. By applying the 3.0 Å cutoff, very uneven axial rises instead of a uniform axial translation were observed for both the XcGyrA-CTD and the EcGyrA-CTD β-pinwheels. Specifically, significant axial rise was only observed between blades 1 and 2, and the axial displacements for all other pairs of adjacent blades (B2–B3, B3–B4, B4–B5, B5–B6) were negligible. This result clearly shows that for XcGyrA-CTD and EcGyrA-CTD blades 2 through 6 form a flat structure; this explains why all the three structures can be superimposed very well by deleting their blade 1s. And the angled packing between blades 1 and 2 is responsible for the overall non-planar architecture.

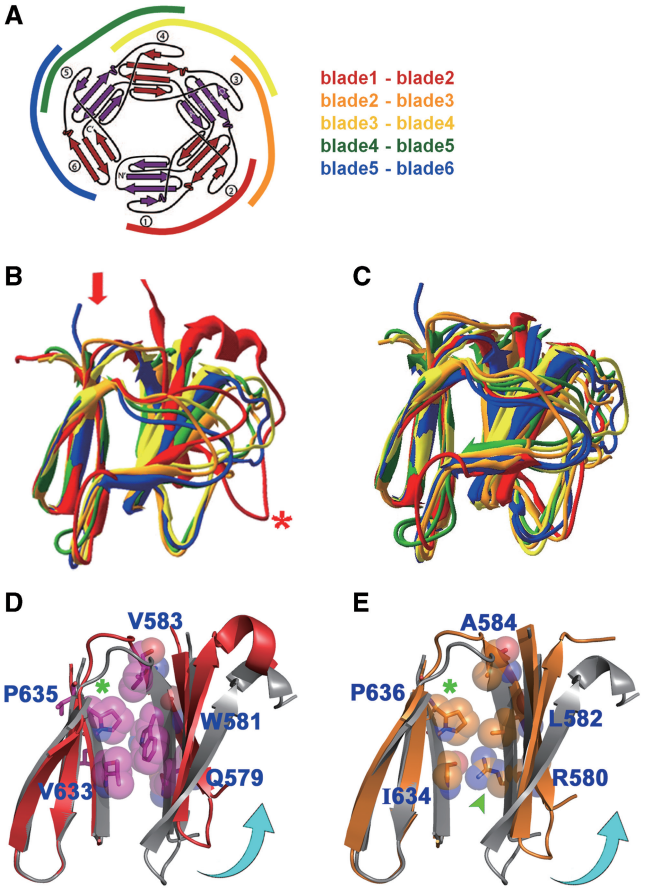

Figure 3. A significant out-of-plane twist is observed between blades 1 and 2 of the canonical GyrA-CTD due to the presence of a conserved β-strand-bearing proline. (**A**) To reveal how the packing between neighboring blades affects the overall structural curvature of GyrA-CTDs, the six blades (B1–B6) of a GyrA-CTD were divided into five adjacent blade pairs: B1–B2 (red), B2–B3 (orange), B3–B4 (yellow), B4–B5 (green) and B5–B6 (blue). The topological diagram was adopted from Ruthenburg *et al.* (13). (**B**) When the C-terminal blades of the XcGyrA-CTD blade pairs (indicated by the red arrow) were superimposed, a significant upward twist on the corresponding N-terminal blade was observed in the B1–B2 pair (highlighted by the red asterisk), whereas all other blade pairs exhibited flat packing. A similar feature was also observed in EcGyrA-CTD (13) (not shown). (**C**) Except for the B1–B2 pair, the remaining blade pairs of XcGyrA-CTD can be aligned nicely with those of BbGyrA-CTD (14), all exhibit flat packing. (**D** and **E**) The B1–B2 pair of BbGyrA-CTD was aligned with that of XcGyrA-CTD (D) and EcGyrA-CTD (E), respectively, by superimposing on blade 2s. Only interface residues from XcGyrA-CTD and EcGyrA-CTD are displayed. In both structures, a β-strand-bearing proline residue (green asterisk) was observed at the penultimate position of the innermost β-strand of blade 2. With its structurally rigid pyrrolidine side-chain pointing toward blade 1, this proline appears to induce an upward twist (indicated by the curved cyan arrows). Note that none of the flat blade pairs has a proline at the corresponding position.

significantly improved when the respective N-terminal β-sheets (blade 1s) were excluded during superposition. This indicates that the remaining portions of the three structures (blades 2–6) are in fact highly similar regardless of the flat or non-planar architecture of the full-length protein. To understand the molecular basis underlying this interesting observation, the 'axial rise' of each β-sheet, as measured by the axial displacement between the two centroids of adjacent β-sheets along the β-pinwheel's central shaft, was characterized. As shown in Table 2, in contrast to some common biological helical structures such as double-helical DNA, α-helices, and various protein filaments that exhibit uniform axial translation between adjacent structural modules, both XcGyrA-CTD and EcGyrA-CTD show very uneven axial displacements. Prominent axial rise is observed only between blades 1 and 2, whereas the packing between all other blade pairs appears relatively planar with negligible axial displacements. Consistently, superposition of adjacent blade pairs clearly revealed the existence of a significant out-of-plane structural twist between blades 1 and 2 (Figure 3B). On the contrary, all other blade pairs exhibit flat packing and can be aligned nicely with those of the BbGyrA-CTD (Figure 3C). Our finding strongly suggests that the planarity of a β-pinwheel structure is linked to the packing geometry between adjacent blades, and that both XcGyrA-CTD and EcGyrA-CTD would be relatively flat without an abrupt spatial rise in blade 1.

This previously unrecognized structural feature of canonical GyrA-CTDs readily explains why the GyrA-box motif is absolutely required for gyrase's unique

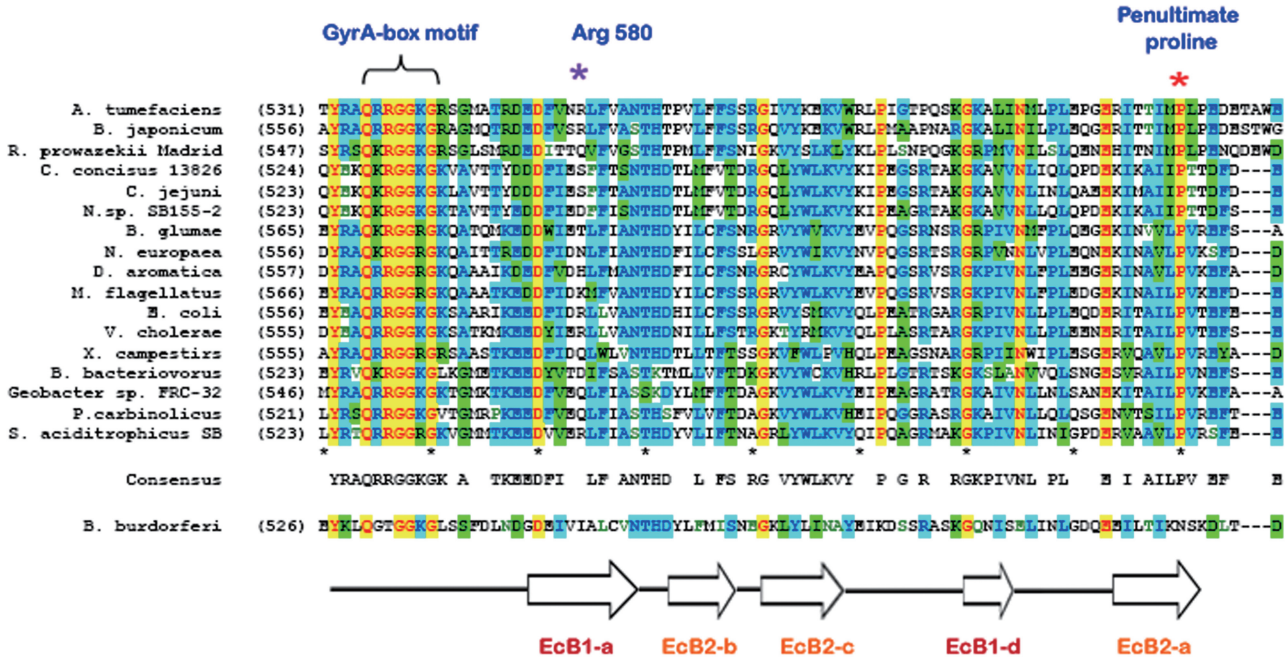

Figure 4. The β-strand-bearing proline is highly conserved among the proteobacterial DNA gyrases. Multiple-alignment of the genomic sequences of GyrA subunits representing the five subdivisions of proteobacteria reveals that the penultimate positioned β-strand-bearing proline following the consensus GyrA-box motif is highly conserved (as indicated by the purple asterisk) among the proteobacteria. The invariant residues are yellow colored, other conserved positions are also colored, with blue and green representing the two most frequently appeared amino acids. Secondary structure assignment were made according to those seen in EcGyrA-CTD (13) and XcGyrA-CTD (arrows represent the β-strands). The sequences of GyrA subunits in the multiple alignment were selected from α-proteobacteria (*Bradyrhizobium japonicum* USDA 110 [BAC49961], *Agrobacterium tumefaciens* str. C58 [AAK87298], *Rickettsia prowazekii* [CAA14671]), β-proteobacteria (*Burkholderia glumae* [BAC98438], *Nitrosomonas europaea* ATCC 19718 [CAD84243], *Methylobacillus flagellatus* KT [YP_545797] and *Dechloromonas aromatica* RCB [YP_284456]), γ-proteobacteria (*Vibrio cholerae* O1 biovar El Tor str. N16961 [AAF94417], *X. campestris* pv. campestris str. ATCC 33913 [NP_636945] and *E. coli* [BAA16048]), δ-proteobacteria (*Geobacter* sp. FRC-32 [ZP_01387645], *Syntrophus aciditrophicus* SB [YP_460051], *Pelobacter carbinolicus* DSM 2380 [YP_355438] and *Bdellovibrio bacteriovorus* HD100 [NP-967035]), ε-proteobacteria (*Nitratiruptor* sp. SB155-2 [YP_001355960], *Campylobacter concisus* 13826 [YP_001466491] and *C. jejuni* subsp. jejuni NCTC 11168 [CAL35145]).

DNA-wrapping and (−) supercoiling activity (11). Because the DNA-contacting canonical GyrA-box motif is located at blade 1 at an end of the curved DNA-binding surface, the markedly angled packing observed between blades 1 and 2 would place blade 1 and the GyrA-box motif at an out-of-plane position relative to the other blades. Consequently, a handed twist is introduced onto the DNA-binding surface (Figure 1B), which allows the bound DNA to be chirally wrapped into a (+) crossover. In the absence of GyrA-box, the remaining DNA binding surface would be relatively flat and is thus incompetent for introducing chiral DNA-wrapping.

The proposed requirement for having DNA-binding residues in blade 1 for gyrase to exhibit (−) supercoiling activity also elucidates why gyrases and those Topo IVs with non-planar and 6-bladed CTD diverge in function. Despite being highly similar in overall structure (13), the DNA-binding surface of 6-bladed BsParC-CTD is largely planar due to the lack of a GyrA-box in its blade 1; which may explain why Topo IVs lack handed DNA-wrapping and (−) supercoiling activities.

A β-strand-bearing proline may define the packing angle between blades 1 and 2

To understand why the packing between blades 1 and 2 of canonical GyrA-CTDs is tilted, the interfaces between all neighboring blades were examined. Unlike interfaces that exhibit flat packing, we noted in both non-planar GyrA-CTDs the presence of a β-strand-bearing proline (Pro636 of EcGyrA-CTD and Pro635 of XcGyrA-CTD) at the penultimate position of blade 2's inner edge β-strand (Figure 3D and E). Located near the hinge that connects blades 1 and 2, the pyrrolidine ring of this proline is constrained by its unique main-chain ϕ angle of −75°, causing it to lie perpendicular to the strand axis and pack against hydrophobic residues from blade 1, seemingly pushing blade 1 away. This structural effect appears to be proline-specific because other amino acids should adopt the typical β-strand ϕ value of −130° at this position, allowing their side-chain atoms beyond Cβ to rotate away from the blade interface without pointing directly toward blade 1, which would favor a flat packing as seen in all other blade pairs. Consistent with its role in defining the tilted packing between blades 1 and 2, a structurally equivalent proline is absent from all other blade interfaces, including those of the flat BbGyrA-CTD. Additionally, this proline is highly conserved among proteobacterial gyrases (Figure 4), but not conserved within Topo IVs with a 6-blade CTD. Thus, the presence of a proline and the tilted packing seen in blade 1 of the BsParC-CTD may simply be an evolutionary remnant.

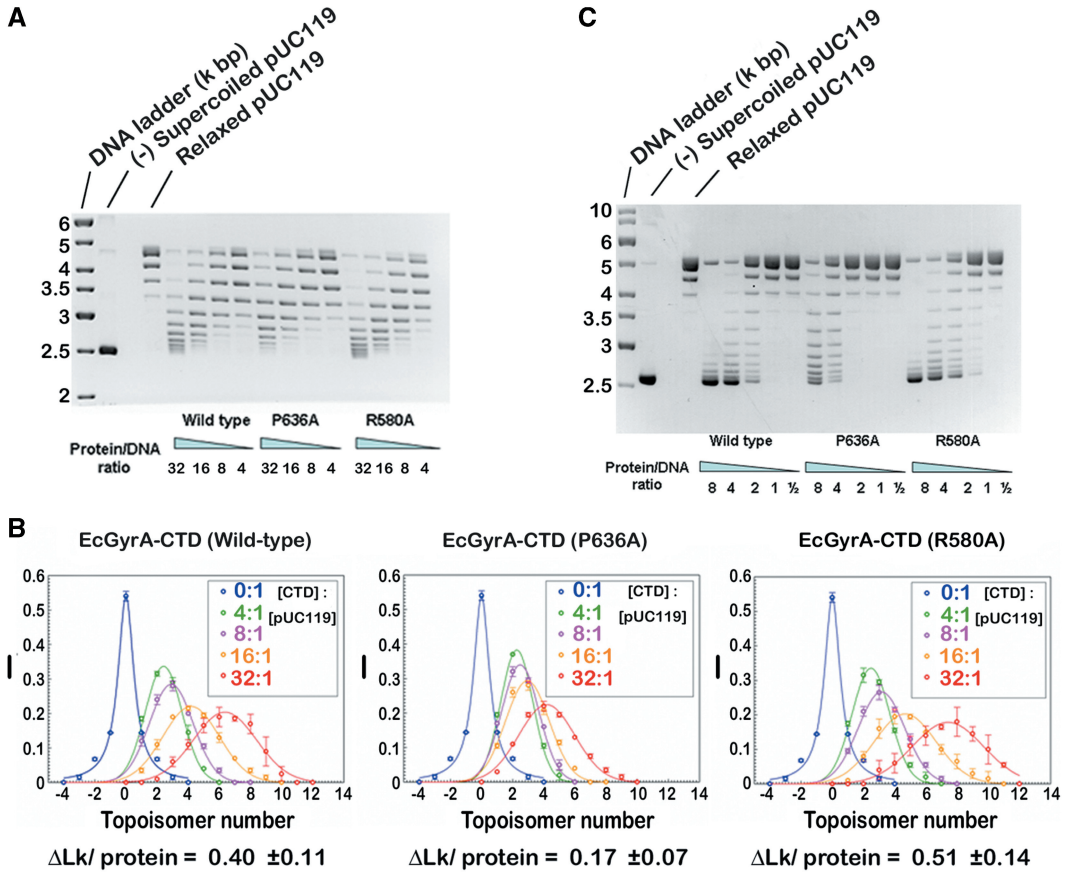

Figure 5. Mutations of the β-strand-bearing proline affect chiral DNA-wrapping by EcGyrA-CTD and the (−) supercoiling activity of gyrase. (**A**) The DNA-wrapping activities of wild-type, P636A and R580A mutant EcGyrA-CTD were examined by the Topo I readout assay (30). Type IB DNA topoisomerase was used to relax plasmid pUC119 in the presence of either wild-type or mutant EcGyrA-CTD, an assay that allows trapping of protein binding-induced changes in DNA superhelicity. The molar ratio of EcGyrA-CTD to plasmid pUC119 (9.6 nM) was indicated. Relaxed and (−) supercoiled pUC119 were included as controls. The DNA-binding affinities of wild-type and mutant proteins were judged to be very similar using a gel-shift assay (Supplementary Figure S2). Moreover, circular dichroism and intrinsic tryptophan fluorescence emission spectra of wild-type and P636A mutant EcGyrA-CTD were measured (Supplementary Figures S3 and S4) to confirm that mutation of P636 to alanine does not globally alter the secondary and tertiary structure of EcGyrA-CTD. (**B**) The relative intensities of topoisomer bands shown in (A) were quantified and fitted to Gaussian curves. The values of the linking number change per protein molecule (ΔL_k/EcGyrA-CTD) were then estimated as described (13). (**C**) DNA supercoiling assay. Relaxed pUC119 plasmid (9.6 M) was incubated with increasing amount (ratio indicated) of wild-type or mutant *E. coli* DNA gyrase. Relaxed and (−) supercoiled pUC119 were included as controls. This assay was also performed at higher enzyme concentration such that larger amount of fully supercoiled species can be produced by the P636A mutant (Supplementary Figure S5). In this figure, three enzyme-to-DNA ratios (2, 4, and 8) overlap those shown in (C), together they provide a wider titration of enzyme concentration (from 0.5 to 16). Results shown in both figures suggest that the P636A mutation reduces gyrase's (−) supercoiling activity by 3–4-fold, as judged by the appearance and relative amount of the fully supercoiled species.

Mutagenesis studies of the β-strand-bearing proline

To test the functional significance directly, a proline to alanine mutation (P636A) was introduced into the EcGyrA-CTD and full-length *E. coli* gyrase. As expected, the P636A mutation clearly impaired the DNA-wrapping activity of EcGyrA-CTD and reduced the supercoiling efficiency of *E. coli* gyrase by 3–4-fold (Figure 5). These data provide evidence that the proline plays a direct role in promoting gyrase's catalytic efficiency by serving as a key structural determinant for the tilted packing between blades 1 and 2, and are consistent with the observation that the non-planar EcGyrA-CTD exhibits stronger DNA-wrapping activity than the proline-less and flat BbGyrA-CTD (13). Given the correlation we observed between DNA-wrapping and supercoiling activity, it is likely that *B. burgdorferi* gyrase possesses a reduced supercoiling activity compared with the *E. coli* enzyme.

Using a mutant *E. coli* gyrase which carries a D82G mutation in the GyrA subunit, it has been shown by microarray analysis that even a 2–3-fold reduction in the negative supercoiling activity leads to drastic changes in the genome-wide gene expression pattern; altering the steady-state transcriptional activity of hundreds of genes (25). Therefore, the 3–4-fold effect caused by the P636A mutation should be functionally significant regarding bacterial physiology.

Notably, mutation of a nearby arginine residue to alanine (R580A) was found to somewhat enhance the DNA-wrapping activity of EcGyrA-CTD (Figure 5A and B); this may have made gyrase a slightly more efficient supercoiling machine (Figure 5C; comparing the lanes of 1:1 molar ratio of protein to DNA). R580 is located at

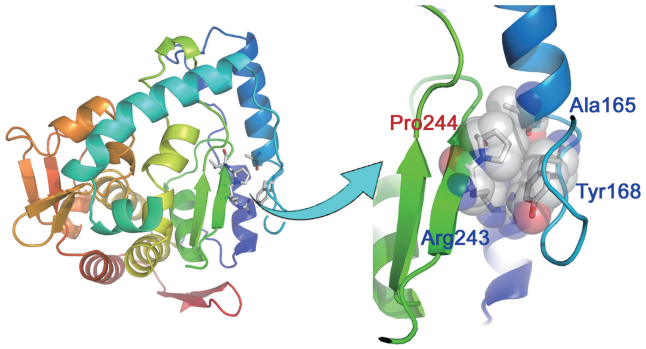

Figure 6. The P244 of phenylalanine hydroxylase [PDB-ID: 1PAH (29)] is also a penultimate β-strand-bearing proline. The P244L mutation is known to impair enzyme activity and cause the genetic disease phenylketonuria, possibly by altering the packing interactions mediated by the pyrrolidine side chain. Residues 211–237 were deleted from the left panel for clarity.

blade 1 of the EcGyrA-CTD. The side-chain of R580 forms van der Waals interactions and a hydrogen bond with groups from blade 2 (Figure 3E), providing a tether between the two blades. Replacement of R580 with alanine abolished these interactions, presumably allowing blade 1 to be pushed further away by P636 and leading to more pronounced blade 1 tilting as well as slightly enhanced DNA-wrapping activity. This finding provides additional support to the tilt-inducing role of P636 and suggests that fine-tuning of gyrase activity can be achieved by modifying the packing geometry between blades 1 and 2.

The β-strand-bearing proline is absent in most singly expressed bacterial type II Topos

Despite the well conserved nature of this β-strand-bearing proline among gyrases (Figure 4), sequence analysis indicated that a structurally equivalent proline is absent in *Mycobacterium tuberculosis* gyrase. As the lone type II Topo in *M. tuberculosis*, the functional characteristics of this enzyme differs from those of the *E. coli* gyrase by exhibiting both (−) supercoiling as well as a significant decatenation activity (26), making it a dual functional enzyme that appears to integrate the properties of both gyrase and Topo IV. It remains to be determined whether this unique feature of *M. tuberculosis* gyrase is shared by other singly expressed bacterial type II Topos. Intriguingly, we noted that the β-strand-bearing proline is also absent in the majority of these lone bacterial type II Topos, including those from *Treponema pallidum* subsp. pallidum SS14 [YP_001933013], *Helicobacter pylori* J99 [NP_223359], *Thermotoga maritima* MSB8 [NP_228890], *Thermoplasma acidophilum* DSM 1728 [NP_394514], *Fervidobacterium nodosum* Rt17-B1 [YP_001410305] and *Thermosipho melanesiensis* BI429 [YP_001306425], with *Petrotoga mobilis* GyrA [YP_001568277] being the only exception. Given the potential role of the β-strand-bearing proline as a modulator of gyrase function, we suspect that the loss of this proline might be one of the molecular events contributing to the functional divergence of *M. tuberculosis* enzyme from canonical DNA gyrase.

Structural and functional significance of β-strand-bearing prolines

Usually, the impact of proline on protein function is discussed in the context of cis-trans isomerization and its role as a secondary structure breaker, the structural and functional effects of β-strand-bearing prolines are to date unrecognized. To our knowledge, this is the first demonstration of a β-strand-bearing proline that may impact protein function. Although proline has the lowest β-strand-forming propensity due to its tightly constrained ϕ angle and its lack of hydrogen on the amide group (27), the following reasons may explain why proline can be accommodated at penultimate position of an edge β-strand. First, this position is not involved in the hydrogen bonding network of β-sheet; thus, the presence of a proline does not cause hydrogen bond loss. Furthermore, larger deviations from the standard main-chain dihedral angles are more common toward the termini of a β-strand; therefore, a proline may be introduced without compromising β-sheet stability. Our finding indicates that site-specific introduction of a penultimate proline into an edge β-strand may alter the local packing interactions, and may thus be a useful protein engineering strategy for modulating protein function.

Medical relevance of β-strand-bearing proline

This work might also have a medical relevance by suggesting a structural basis for the disease-causing P244L mutation in phenylalanine hydroxylase (28), an enzyme catalyzes the conversion of phenylalanine to tyrosine. Deficiency or reduction in this enzymatic activity causes accumulation of phenylalanine and phenylketone, leading to the disease phenylketonuria. Similar to P636 of *E. coli* GyrA subunit, we found that P244 of phenylalanine hydroxylase is also located at the penultimate position of a β-strand with a ϕ angle of −75° (Figure 6) (29). The P244L substitution is expected to affect the protein structure by altering pyrrolidine-mediated packing interactions, which explains the observed reduction in enzyme activity and consequently phenylketonuria (28).

ACCESSION NUMBER

Coordinates and structure factors for XcGyrA-CTD have been deposited to Protein Data Bank with accession code 3L6V.

SUPPLEMENTARY DATA

Supplementary Data are available at NAR Online.

ACKNOWLEDGEMENTS

We thank Drs Tony Maxwell, Hiroshi Hiasa, Tao-Shih Hsieh, Andrew Wang, Yu-Jen Yu, Xin Chen and Tsai-Kun Li for discussion and critical reading of the manuscript and Li-Ying Lin, Chyun-Chuan Wu and Yu-Yung Chang for technical assistance. Portions of this research were carried out at beamline BL13B1 of the

National Synchrotron Radiation Research Center (Taiwan) and beamline SP12B2 of the SPring8 (Japan).

FUNDING

The National Science Council [grant number NSC96-2113-M-002-022-MY3]; National Research Program for Genomic Medicine [grant number NSC97-3112-B-002-048] (to N.-L.C.). Funding for open access charge: National Science Council (Taiwan).

Conflict of interest statement. None declared.

REFERENCES

1. Schoeffler,A.J. and Berger,J.M. (2008) DNA topoisomerases: harnessing and constraining energy to govern chromosome topology. *Q. Rev. Biophys.*, **41**, 41–101.
2. Champoux,J.J. (2001) DNA topoisomerases: structure, function, and mechanism. *Annu. Rev. Biochem.*, **70**, 369–413.
3. Wang,J.C. (2002) Cellular roles of DNA topoisomerases: a molecular perspective. *Nat. Rev. Mol. Cell Biol.*, **3**, 430–440.
4. Peng,H. and Marians,K.J. (1995) The interaction of Escherichia coli topoisomerase IV with DNA. *J. Biol. Chem.*, **270**, 25286–25290.
5. Lee,M.P., Sander,M. and Hsieh,T. (1989) Nuclease protection by Drosophila DNA topoisomerase II. Enzyme/DNA contacts at the strong topoisomerase II cleavage sites. *J. Biol. Chem.*, **264**, 21779–21787.
6. Liu,L.F. and Wang,J.C. (1978) DNA-DNA gyrase complex: the wrapping of the DNA duplex outside the enzyme. *Cell*, **15**, 979–984.
7. Brown,P.O. and Cozzarelli,N.R. (1979) A sign inversion mechanism for enzymatic supercoiling of DNA. *Science*, **206**, 1081–1083.
8. Higgins,N.P., Peebles,C.L., Sugino,A. and Cozzarelli,N.R. (1978) Purification of subunits of Escherichia coli DNA gyrase and reconstitution of enzymatic activity. *Proc. Natl Acad. Sci. USA*, **75**, 1773–1777.
9. Reece,R.J. and Maxwell,A. (1991) The C-terminal domain of the Escherichia coli DNA gyrase A subunit is a DNA-binding protein. *Nucleic Acids Res.*, **19**, 1399–1405.
10. Kampranis,S.C. and Maxwell,A. (1996) Conversion of DNA gyrase into a conventional type II topoisomerase. *Proc. Natl Acad. Sci. USA*, **93**, 14416–14421.
11. Kramlinger,V.M. and Hiasa,H. (2006) The ''GyrA-box'' is required for the ability of DNA gyrase to wrap DNA and catalyze the supercoiling reaction. *J. Biol. Chem.*, **281**, 3738–3742.
12. Ward,D. and Newton,A. (1997) Requirement of topoisomerase IV parC and parE genes for cell cycle progression and developmental regulation in Caulobacter crescentus. *Mol. Microbiol.*, **26**, 897–910.
13. Ruthenburg,A.J., Graybosch,D.M., Huetsch,J.C. and Verdine,G.L. (2005) A superhelical spiral in the Escherichia coli DNA gyrase A C-terminal domain imparts unidirectional supercoiling bias. *J. Biol. Chem.*, **280**, 26177–26184.
14. Corbett,K.D., Shultzaberger,R.K. and Berger,J.M. (2004) The C-terminal domain of DNA gyrase A adopts a DNA-bending beta-pinwheel fold. *Proc. Natl Acad. Sci. USA*, **101**, 7293–7298.
15. Hsieh,T.J., Farh,L., Huang,W.M. and Chan,N.L. (2004) Structure of the topoisomerase IV C-terminal domain: a broken beta-propeller implies a role as geometry facilitator in catalysis. *J. Biol. Chem.*, **279**, 55587–55593.
16. Ramakrishnan,V., Finch,J.T., Graziano,V., Lee,P.L. and Sweet,R.M. (1993) Crystal structure of globular domain of histone H5 and its implications for nucleosome binding. *Nature*, **362**, 219–223.
17. Otwinowski,Z. and Minor,W. (1997) *Methods Enzymol.,* Vol. 276, Academic Press, London, UK, pp. 307–326.
18. Terwilliger,T.C. and Berendzen,J. (1999) Automated MAD and MIR structure solution. *Acta Crystallogr. D Biol. Crystallogr.*, **55**, 849–861.
19. Terwilliger,T.C. (2000) Maximum-likelihood density modification. *Acta Crystallogr. D Biol. Crystallogr.*, **56**, 965–972.
20. Terwilliger,T.C. (2003) Automated main-chain model building by template matching and iterative fragment extension. *Acta Crystallogr. D Biol. Crystallogr.*, **59**, 38–44.
21. Terwilliger,T.C. (2003) Automated side-chain model building and sequence assignment by template matching. *Acta Crystallogr. D Biol. Crystallogr.*, **59**, 45–49.
22. Jones,T.A., Zou,J.Y., Cowan,S.W. and Kjeldgaard,M. (1991) Improved methods for building protein models in electron density maps and the location of errors in these models. *Acta Crystallogr. A*, **47 (Pt 2)**, 110–119.
23. Collaborative Computational Project, N. (1994) The CCP4 suite: programs for protein crystallography. *Acta Crystallog. D*, 764–767.
24. Klungsoyr,H.K. and Skarstad,K. (2004) Positive supercoiling is generated in the presence of Escherichia coli SeqA protein. *Mol. Microbiol.*, **54**, 123–131.
25. Jeong,K.S., Ahn,J. and Khodursky,A.B. (2004) Spatial patterns of transcriptional activity in the chromosome of Escherichia coli. *Genome Biol.*, **5**, R86.
26. Aubry,A., Fisher,L.M., Jarlier,V. and Cambau,E. (2006) First functional characterization of a singly expressed bacterial type II topoisomerase: the enzyme from Mycobacterium tuberculosis. *Biochem. Biophys. Res. Commun.*, **348**, 158–165.
27. Minor,D.L. Jr and Kim,P.S. (1994) Measurement of the beta-sheet-forming propensities of amino acids. *Nature*, **367**, 660–663.
28. Perez,B., Desviat,L.R., Gomez-Puertas,P., Martinez,A., Stevens,R.C. and Ugarte,M. (2005) Kinetic and stability analysis of PKU mutations identified in BH4-responsive patients. *Mol. Genet. Metab.*, **86(Suppl. 1)**, S11–16.
29. Erlandsen,H., Fusetti,F., Martinez,A., Hough,E., Flatmark,T. and Stevens,R.C. (1997) Crystal structure of the catalytic domain of human phenylalanine hydroxylase reveals the structural basis for phenylketonuria. *Nat. Struct. Biol.*, **4**, 995–1000.
30. Musgrave,D.R., Sandman,K.M. and Reeve,J.N. (1991) DNA binding by the archaeal histone HMf results in positive supercoiling. *Proc. Natl Acad. Sci. USA*, **88**, 10397–10401.